

Propagation and control of nano-scale magnetic droplet solitons

M. A. Hofer^{1,*} M. Sommacal^{1,†} and T. J. Silva^{2,‡}

¹*Department of Mathematics, North Carolina State University, Raleigh, North Carolina 27695, USA*

²*National Institute of Standards and Technology, Boulder, Colorado 80305, USA*

(Dated: September 22, 2018)

The propagation and controlled manipulation of strongly nonlinear, two-dimensional solitonic states in a thin, anisotropic ferromagnet are theoretically demonstrated. It has been recently proposed that spin-polarized currents in a nanocontact device could be used to nucleate a stationary dissipative droplet soliton. Here, an external magnetic field is introduced to accelerate and control the propagation of the soliton in a lossy medium. Soliton perturbation theory corroborated by two-dimensional micromagnetic simulations predicts several intriguing physical effects, including the acceleration of a stationary soliton by a magnetic field gradient, the stabilization of a stationary droplet by a uniform control field in the absence of spin torque, and the ability to control the soliton's speed by use of a time-varying, spatially uniform external field. Soliton propagation distances approach 10 μm in low loss media, suggesting that droplet solitons could be viable information carriers in future spintronic applications, analogous to optical solitons in fiber optic communications.

I. INTRODUCTION

Nanomagnetism holds great promise for future spin-based information storage and processing technologies¹. One enabling physical effect is spin torque², which imparts angular momentum from a spin-polarized current to a magnet. Spin torque forms the basis for tunable microwave nano-oscillators in *confined* nanopillar structures³ and nanocontacts abutting an *extended* ferromagnet⁴. Most nanopillar dynamics can be reasonably described by single-domain modeling⁵ with the notable exception of gyrotropic vortex motion⁶. In contrast, nanocontacts enable the excitation of radiating^{7–9} and localized, coherently precessing, nonlinear wave states⁸. The analysis of solitonic waves in nanocontact systems has predominantly been limited to either the weakly nonlinear regime at threshold¹⁰ or complex micromagnetic simulations^{5,11}.

We recently proposed that a spin torque driven nanocontact could act as a soliton creator in a uniaxial ferromagnet with sufficiently strong perpendicular anisotropy¹². The resultant strongly nonlinear, coherently precessing state was termed a dissipative droplet soliton, the locally driven/uniformly damped cousin of the two-dimensional, nontopological droplet soliton¹³. Prior numerical computations suggested that the conservative, stationary droplet could be generalized to a propagating solution¹⁴. Small amplitude droplets were then shown to propagate as approximate, Nonlinear Schrödinger bright solitons in [15]. The construction and properties of a stable, two-parameter family of large amplitude propagating droplet solutions in a lossless medium was undertaken in [16]. However, a viable method to accelerate solitons and understand their propagation in physically realistic, damped media is lacking.

In this work, we use soliton perturbation theory to semi-analytically demonstrate the feasibility of sustaining, moving, and controlling a droplet soliton in a damped medium solely under the action of an external magnetic field. Modulation equations describing the evo-

lution of the soliton's speed and precessional frequency in the presence of damping and a temporally/spatially varying external field are studied and the results are corroborated by 2D micromagnetic simulations. We show that a stationary droplet can be accelerated by a field gradient. Once in motion, the soliton's speed can be controlled by a spatially uniform, time-varying external field. A field gradient due to two nanowires can accelerate a soliton to propagate approximately 10 μm in a low loss ferromagnet. Stationary droplets of any allowable frequency can be created from a sufficiently large, localized magnetic excitation, induced by a nanocontact or otherwise, and then stabilized by a linear feedback control field without the use of spin torque. This represents a new mechanism to study magnetic solitons without strong, spin torque induced perturbations. Analogous to optical solitons in fiber-optic telecommunications¹⁷, these results show that droplet solitons act as stable, controllable, particle-like, precessing dipoles that exhibit intriguing nonlinear physics and hold potential for spintronic applications.

The layout of this work is as follows. First, we introduce the model equations and then proceed with the finite dimensional reduction via soliton perturbation theory. The reduced system enables a thorough analysis of droplet dynamics under the influence of damping and a spatio-temporal magnetic field undertaken in the next section. Two control mechanisms, feedback control of a stationary droplet's frequency and open loop control of a propagating droplet's speed, are then introduced. We conclude with some discussion and future outlook.

II. MODEL

The model of magnetization dynamics we consider is the Landau-Lifshitz equation⁵

$$\begin{aligned}\frac{\partial \vec{m}}{\partial t} &= -\vec{m} \times \vec{h}_{\text{eff}} - \alpha \vec{m} \times (\vec{m} \times \vec{h}_{\text{eff}}) \\ \vec{h}_{\text{eff}} &= \nabla^2 \vec{m} + (h_0 + m_z) \hat{z},\end{aligned}\quad (1)$$

describing a thin, two-dimensional, unbounded, damped ($\alpha > 0$ is the damping parameter) ferromagnet. The effective field incorporates exchange $\nabla^2 \vec{m}$, an external magnetic field $h_0(\vec{x}, t)\hat{z}$ pointing in the perpendicular direction normal to the film plane, and perpendicular anisotropy $m_z \hat{z}$. Crystalline anisotropy, characterized by the anisotropy field H_k , is assumed sufficient to overcome the local demagnetizing field so that $H_k > M_s$. Time, space, and fields are normalized by scaled versions of the Larmor frequency $|\gamma|\mu_0 M_s(Q-1)$, exchange length $L_{\text{ex}}/\sqrt{Q-1}$, and saturation magnetization $M_s(Q-1)$, respectively, where $Q = H_k/M_s > 1$. We note that for the solitons studied here, the magnetostatic field is approximately local for films with thickness much smaller than $L_{\text{ex}}/\sqrt{Q-1}$ (see discussion in¹⁶). For Co/Ni multilayer anisotropic ferromagnets used in recent experiments¹⁸, the temporal scale and length scale are approximately 27 ps and 17 nm, respectively, and $\alpha \approx 0.01$, $Q \approx 1.25$, $M_s \approx 650$ kA/m. References to dimensional results use these parameter values.

In what follows, we assume that a localized excitation of large amplitude has been nucleated by a spin torque nanocontact¹² or some other means. The rest of this work is concerned with the manipulation of this structure in a lossy medium by use of an external field.

When $h_0 = \alpha = 0$, eq. (1) admits the conservation of total spin, momentum, and energy

$$\begin{aligned}\mathcal{N} &= \int (1 - \cos \Theta) d\vec{x}, \\ \vec{\mathcal{P}} &= \int (\cos \Theta - 1) \nabla \Phi d\vec{x}, \\ \mathcal{E}_0 &= \frac{1}{2} \int [|\nabla \Theta|^2 + \sin^2 \Theta (1 + |\nabla \Phi|^2)] d\vec{x},\end{aligned}$$

respectively, where all integrals are taken over the plane and Θ , Φ are the polar and azimuthal angles of the magnetization, respectively. Minimizing the energy subject to fixed \mathcal{N} and $\vec{\mathcal{P}}$ leads to a two-parameter family of localized, precessing, stable traveling waves called propagating droplet solitons parameterized by their velocity \vec{V} and frequency in the comoving frame ω ¹⁶. There is a bijective map from $(\mathcal{N}, \vec{\mathcal{P}})$ to the physical parameters (ω, \vec{V}) . Droplet localization requires that the velocity and frequency of the propagating droplet lie below the spin wave band, enforcing the restriction¹³

$$\begin{aligned}\omega + |\vec{V}|^2/4 < 1, \quad \vec{V} \neq 0, \\ 0 < \omega < 1, \quad \vec{V} = 0.\end{aligned}\tag{2}$$

We note that it is possible for moving droplets to exhibit negative rest frequencies $\omega < 0$ ¹⁶. Typical droplet widths are of order one, hence are nanoscale excitations. Stationary droplets with rest frequencies close to zero resemble static circular bubbles, which received a great deal of attention in the past¹⁹. However, typical bubble sizes are much larger. With the inclusion of nonlocal magnetostatic fields, Thiele [20] predicted that a static

bubble will be stable for a 5 nm thick film with a radius above 63 μm . Thus, droplets can be viewed as smaller, dynamic generalizations of the static bubble.

Allowing for weak damping ($\alpha \ll 1$) and a slowly varying magnetic field ($|\nabla h_0|, |\partial_t h_0| \ll 1$), with no restriction on the magnitude of h_0 , causes the total spin, momentum, and energy to evolve in time. Through the map to (ω, \vec{V}) , we can describe the droplet's adiabatic, particle-like evolution by a time dependence of the droplet's velocity and rest frequency, trajectories in the V - ω phase plane.

III. FINITE DIMENSIONAL REDUCTION

Using soliton perturbation theory (see, e.g., [21]), we obtain the following finite dimensional system of modulation equations describing the slow modulation of the total spin and momentum:

$$\begin{aligned}\frac{d\mathcal{N}}{dt} &= -\alpha(\omega + h_0) \int \sin^2 \Theta d\vec{x} \\ &\quad - \alpha \vec{V} \cdot \int \sin^2 \Theta \nabla \Phi d\vec{x},\end{aligned}\tag{3a}$$

$$\begin{aligned}\frac{d\vec{\mathcal{P}}}{dt} &= -\nabla h_0 \mathcal{N} + \alpha(\omega + h_0) \int \sin^2 \Theta \nabla \Phi d\vec{x} \\ &\quad - \alpha \vec{V} \cdot \int (\nabla \Phi \sin^2 \Theta \nabla \Phi + \nabla \Theta \nabla \Theta) d\vec{x}.\end{aligned}\tag{3b}$$

The energy $\mathcal{E} = \mathcal{E}_0 + \frac{1}{2} \int h_0 (1 - \cos \Theta) d\vec{x}$ is constrained to evolve according to

$$\frac{d\mathcal{E}}{dt} = (\omega + h_0) \frac{d\mathcal{N}}{dt} + (\partial_t h_0 + \vec{V} \cdot \nabla h_0) \mathcal{N} + \vec{V} \cdot \frac{d\vec{\mathcal{P}}}{dt};\tag{4}$$

thus, it is sufficient to evolve eqs. (3) only. The integrals are evaluated with conservative droplets (Θ, Φ) of given total spin $\mathcal{N}(t)$ and momentum $\vec{\mathcal{P}}(t)$ or, equivalently, rest frequency $\omega(t)$ and velocity $\vec{V}(t)$. The slowly varying field is evaluated along the soliton trajectory $h_0 = h_0(\vec{X}(t), t)$, where $d\vec{X}/dt = \vec{V}$. Similar modulation equations were derived for one-dimensional droplets in [22–24] and stationary, two-dimensional droplets ($\vec{\mathcal{P}} \equiv 0$) in [24]. Without loss of generality, we limit further discussion to droplet motion in the x direction, so that $\vec{V} = (V, 0)$ and $\vec{\mathcal{P}} = (\mathcal{P}, 0)$.

In [16], we numerically computed a library of propagating droplets using an iterative technique²⁶. These precomputed states are used here to numerically solve the modulation equations (3) and to recover $\omega(t)$ and $V(t)$. The initial value problem for eqs. (3) is numerically solved with initial parameters (V_0, ω_0) chosen inside the precomputed library²⁶. Interpolants mapping $(\mathcal{N}, \mathcal{P})$ to (V, ω) and vice-versa as well as for the integrals in (3) are generated from the droplet library. We then numerically evolve eqs. (3) in time using the interpolants. We also perform micromagnetic simulations of eq. (1) by use of a

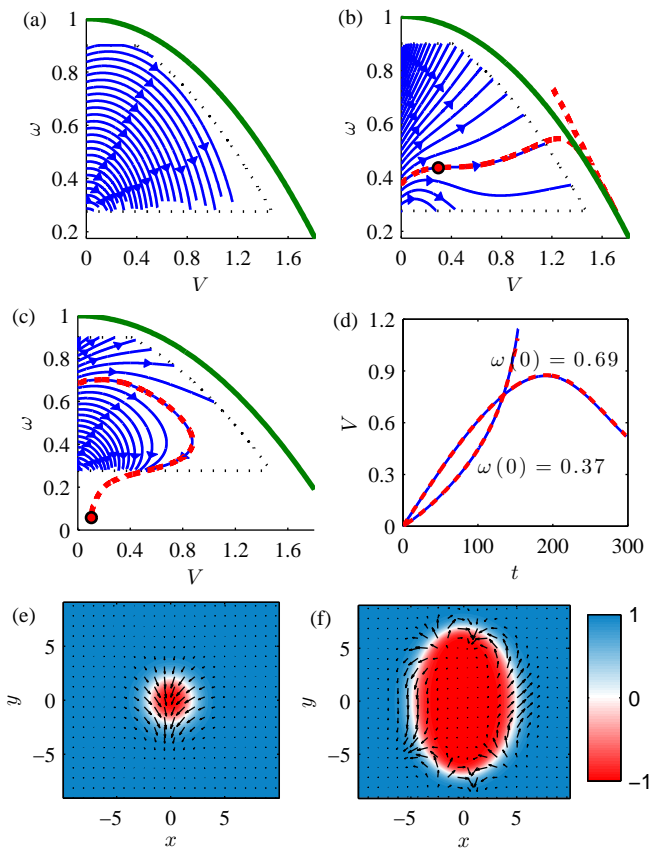


FIG. 1. (a,b,c) Droplet trajectories in the V - ω plane from numerical integration of the modulation equations (3) (solid) and micromagnetics (dashed). The dotted curves correspond to the edges of the precomputed droplet library and the thick, solid parabolic curve is the spin wave band. (a) low loss $\alpha = 0.001$. (b) $\alpha = 0.01$, positive bias field. (c) $\alpha = 0.01$, negative bias field. See text for further details. (d) Droplet velocity time dependence for the solid/dashed trajectories in (b,c). (e,f) Droplet profiles from micromagnetics corresponding to the circles in (b,c), respectively. The gray (color) scale represents the out-of-plane magnetization m_z and the arrows represent the in-plane components.

pseudospectral method¹⁶. To recover the micromagnetic solution's speed and frequency, we compute the center of mass $\int \vec{x}(1 - \cos\Theta) d\vec{x}/\mathcal{N}$ and the phase at the center of mass at each time step. The velocity and comoving frequency are then found by differentiation. The rest frequency is recovered by subtracting the local magnetic field $h_0(\vec{X}(t), t)$.

The modulation eqs. (3) represent a low dimensional projection of the magnetodynamics enabling us to bring finite-dimensional dynamical systems methods and control theory to bear on the problem. As we will demonstrate, the results from modulation theory agree exceptionally well with micromagnetics.

IV. DROPLET SOLITON DYNAMICS

The dynamics of eqs. (3) depend on the magnitude of $|\nabla h_0|/\alpha$. We consider each regime in turn.

A. Negligible Damping: $|\nabla h_0/\alpha| \gg 1$

When $|\nabla h_0/\alpha| \gg 1$, the total spin is approximately conserved and the momentum varies. The V - ω phase plane for $h_0 = 0.5 - 0.005x$ and $\alpha = 0.001$ pictured in Fig. 1(a) closely resembles trajectories of constant total spin, $\mathcal{N} = \mathcal{N}_0$ or constant energy depicted in [16]. These low damping dynamics can be approximated by setting $\alpha = 0$. Then eqs. (9) and (11) become Newton's law

$$d\vec{\mathcal{P}}/dt = -\mathcal{N}_0 \nabla h_0(\vec{X}, t), \quad d\vec{X}/dt = \vec{V},$$

for the motion of the soliton center $\vec{X}(t)$ subject to the potential $\mathcal{N}_0 h_0$. Thus, engineering the magnetic field in an appropriate way allows one to control the motion of the particle-like soliton. Note that the effective mass

$$m_{\text{eff}}(\omega, V) = \frac{\mathcal{P}(\omega, V)}{V}, \quad (5)$$

depends on the soliton speed and frequency. The stationary droplet is accelerated while the rest frequency decreases, representing a transfer of the effective potential energy stored in the precessional motion ω to effective kinetic energy of translational motion V .

B. Comparable Damping and Field Gradient: $|\nabla h_0/\alpha| = \mathcal{O}(1)$

For the balance $|\nabla h_0/\alpha| = \mathcal{O}(1)$, different dynamics occur. Figure 1(b) depicts trajectories for the same field as in 1(a) but with and order of magnitude larger damping $\alpha = 0.01$. The dashed curve depicts the trajectory from micromagnetics with $\omega(0) = 0.37$. The circle on this trajectory corresponds to the droplet shown in Fig. 1(e). The droplet is accelerated and is accompanied by an amplitude decrease until it devolves into a linear spin wave upon reaching the band edge (eq. (2)). The micromagnetic simulation closely matches the adiabatic theory until the band edge is reached and the solution amplitude is very small, after which the droplet ansatz is no longer valid. A plot of $V(t)$ is shown in Fig. 1(d).

During the course of evolution, a droplet can experience deceleration, as in Fig. 1(c) with $\alpha = 0.01$ and a negative bias field, $h_0 = -0.5 - 0.005x$. This behavior is reminiscent of Bloch oscillations predicted for one-dimensional droplets in [23]. In the one-dimensional (1D) case, the soliton oscillates under a constant force. We have not observed such behavior in our micromagnetic simulations or in the modulation theory. Instead, simulations reveal the formation of local, topological structure including vortex/anti-vortex pairs and what appears

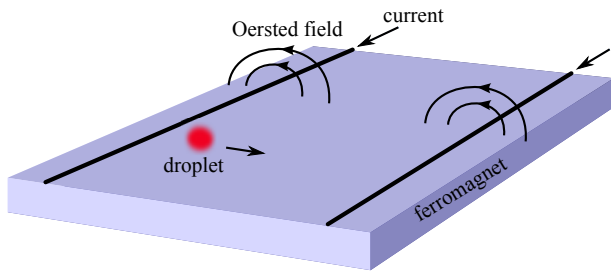


FIG. 2. Droplet acceleration by current flowing through two nanowires.

to be switching of the magnetization to the inverted, $\Theta \equiv \pi$ state, corresponding to $(V, \omega) = (0, 0)$ shown in Fig. 1(f). Previous work on solitons in *isotropic* ferromagnets reveal the existence of nontopological droplets bifurcating into co-propagating vortex, anti-vortex pairs when a critical momentum is reached²⁵. Approximate vortex, anti-vortex pairs were studied in the anisotropic case numerically¹⁴ but have not been observed in our micromagnetic studies here.

In addition to the dynamics of Fig. 1 for constant field gradient, we have also simulated droplet acceleration due to the field generated by two current-carrying nanowires in the plane of the film with current in the same direction and a stationary droplet nucleated in between them (Fig. 2). The current induced Oersted fields lead to a negative magnetic field gradient that accelerates the droplet. The low dimensional modulation system, eq. (3), enables a detailed investigation of parameter space that would, using micromagnetic simulations, be prohibitive to explore. The simulations incorporate the Oersted field due to two infinite wires with 150 nm diameters and varying separation. Stationary droplets with varying frequencies are assumed to be nucleated 300 nm from the center of the left wire and allowed to propagate until either reaching the second wire or the soliton center of mass attains the value $m_z = 0.5$. For the moderate damping case $\alpha = 0.01$, the droplet is predicted to travel up to $3 \mu\text{m}$ in about 30 ns for 15 mA current in each wire with a $3.3 \mu\text{m}$ wire separation. Top speeds can approach 600 m/s. In the low-loss case $\alpha = 0.001$, the droplet can propagate about $10 \mu\text{m}$ in 70 ns for a 10 mA current with a $10.3 \mu\text{m}$ wire separation.

C. Negligible Field Gradient: $|\nabla h_0|/\alpha \ll 1$

The remaining regime, when $|\nabla h_0|/\alpha \ll 1$, is now investigated. We focus on the case of a uniform and static magnetic field, assuming that a propagating droplet has been created. In Fig. 3, solution of the modulation system (3) reveals the *acceleration* of a propagating droplet due to damping when the magnetic field is zero or positive. When the field is sufficiently negative, the droplet can experience deceleration and then acceleration as its amplitude decays. This counter-intuitive droplet accel-

eration due to damping was predicted for 1D droplets in the absence of a magnetic field²². We can understand this behavior in terms of the droplet's effective mass (5). From eq. (5) we have $\dot{P} = \dot{m}_{\text{eff}}V + m_{\text{eff}}\dot{V}$ where $\dot{\cdot}$ denotes time differentiation. In the absence of a field gradient, eq. (11) implies a decrease in momentum $\dot{P} < 0$. Then a droplet can be accelerated ($\dot{V} > 0$) if

$$\dot{m}_{\text{eff}} < \dot{P}/V < 0. \quad (6)$$

In other words, the droplet is accelerated in the presence of damping because the effective mass is decreasing at a sufficiently fast rate.

As shown in Fig. 3(b), inequality (6) holds for $\omega > 0.3$ and positive fields. When $-1 < h_0 < 0$, there are some droplets that exhibit deceleration. In this case, the magnet undergoes a complete reversal to the $(V, \omega) = (0, 0)$ state for initial droplets with parameters lying below a separatrix (see Fig. 3(c)) which we term the *switching separatrix*. The switching separatrix corresponds to the stable manifold of the fixed point $(V, \omega) = (0, -h_0)$. Linearization of eqs. (3) around this fixed point results in the eigenvalues

$$\left(\frac{-\int \sin^2 \Theta d\vec{x}}{\partial_\omega \mathcal{N}}, \quad \frac{-\int \Theta_x^2 d\vec{x}}{\partial_V \mathcal{P}} \right), \quad (7)$$

evaluated at $(V, \omega) = (0, -h_0)$. Since $\partial_\omega \mathcal{N} < 0$ ¹³ and $\partial_V \mathcal{P} > 0$ for stationary droplets, the fixed point is a saddle. The switching separatrix from modulation theory accurately resolves the micromagnetic dynamics as evidenced by the close agreement in Fig. 3(c) for trajectories starting very close to the separatrix. The switching separatrix for negative bias field leads to the differing phase plane trajectories in Figs. 1(b) and (c). Physically, this analysis reveals that there is a synergy between damping and the bias field. A bias above $-\omega$ leads to a decrease of the soliton amplitude whereas a bias below causes an increase in soliton amplitude. This suggests a mechanism for stabilizing a stationary droplet at the saddle point $(V, \omega) = (0, -h_0)$ by dynamically changing the bias field with feedback control.

V. DROPLET SOLITON CONTROL

A. Stationary Droplet Stabilization

The nucleation of a stationary droplet by a spin torque driven nanocontact has been theoretically demonstrated¹². The droplet, which would otherwise decay due to damping, is sustained by a balance between localized driving and uniform damping. However, the current-induced Oersted field strongly perturbs the stationary droplet from its ideal, symmetric structure, leading to phase variations and potentially a drift instability whereby the droplet is ejected from the nanocontact¹². Furthermore, canting of the polarization layer is required

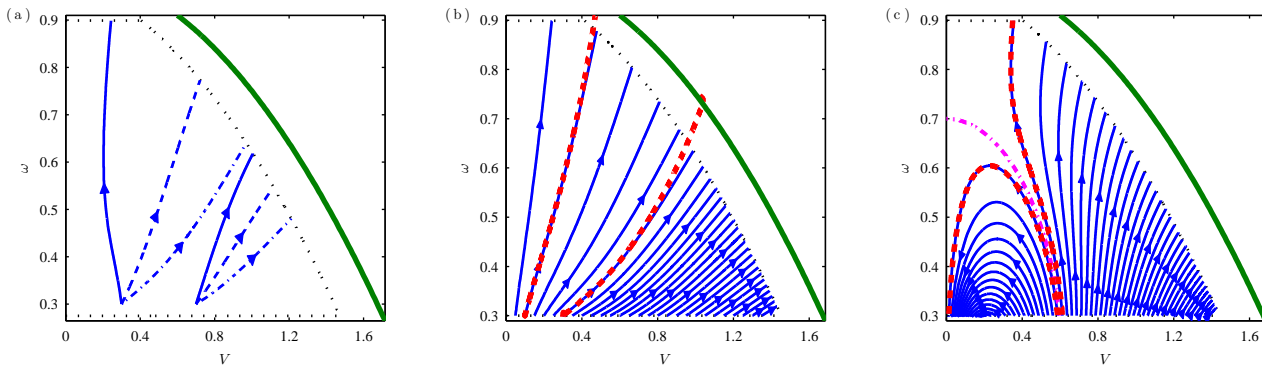


FIG. 3. Droplet trajectories with uniform, static magnetic field and $\alpha = 0.01$. (a) Modulation solution showing acceleration or deceleration of a propagating droplet due to damping and $h_0 = -0.4$ (solid), $h_0 = 0$ (dashed), and $h_0 = 0.9$ (dash-dotted). (b) $h_0 = 1$. (c) $h_0 = -0.7$. In (b) and (c), the dashed curves are micromagnetic simulations. In (c), the dash-dotted curve is the separatrix between the switched state $(V, \omega) = (0, 0)$ and spin wave states.

to obtain an ac electrical signal via giant magnetoresistance leading to symmetry breaking of the spin torque term and further complexity. We propose a simple alternative stabilizing mechanism that avoids these difficulties: a closed-loop, spatially uniform control field. The stationary droplet saddle point $(V, \omega) = (0, \omega_*)$ for $h_0 = -\omega_*$ and $0 < \omega_* < 1$ is altered to an attractor by introducing the linear feedback control

$$h_0(t) = -\omega_* + G\Omega(t), \quad (8)$$

with gain G , bias $-\omega_*$, and the total, measured system frequency $\Omega(t) = \omega(t) + h_0(t)$. Feedback implementation could be realized by use of a small amplitude (sub-threshold) dc current applied to a trilayer nanocontact with a canted fixed layer, resulting in a measurement of Ω with negligible spin torque and Oersted field effects. Another possibility is direct imaging of the dynamics.

The goal is to drive Ω to zero. With such a control law, linearization of eq. (3) around the fixed point results in the eigenvalues

$$\left(\frac{\int \sin^2 \Theta d\vec{x}}{(G-1)\partial_\omega \mathcal{N}}, \quad \frac{-\int \Theta_x^2 d\vec{x}}{\partial_V \mathcal{P}} \right). \quad (9)$$

Since $\partial_\omega \mathcal{N} < 0$ and $\partial_V \mathcal{P} > 0$ ¹⁶, when $G > 1$ both eigenvalues are negative and the fixed point is linearly stable. This proves linear stability. However, if the initial system frequency is too close to 1, one may apply the feedback field (8) with $h_0 < -1$ leading to spontaneous reversal of the magnetic film. To avoid this scenario and stabilize the droplet, the gain is restricted to

$$G > \max(1, 1 + \omega(0) - \omega_*).$$

The gain G determines the relaxation rate to the fixed point, with larger values leading to slower relaxation. For excitations with $\omega(0) - \omega_* > 0$, G cannot be very close to 1. Thus, there is a trade-off between the relaxation time and the stability of the ferromagnet.

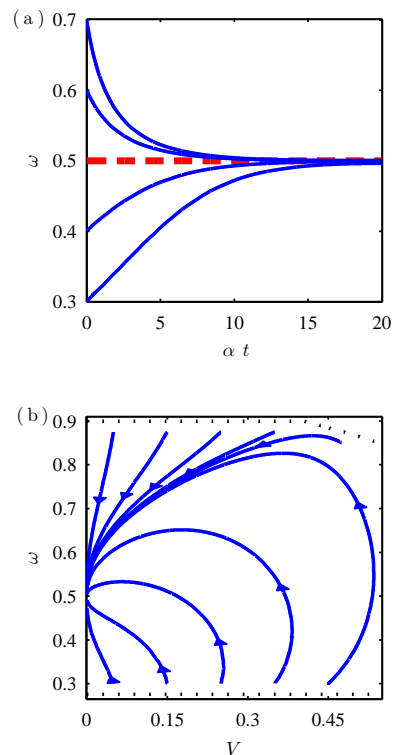


FIG. 4. Stabilization of a stationary droplet with $\omega_* = 0.5$ by the linear feedback control law (8) with $G = 2$. (a) Stationary droplet relaxation. (b) Trajectories in the V - ω plane.

We observe that the fixed point is a global attractor of the modulation equations (3) in Fig. 4. Figure 4(a) shows the relaxation of the frequency to $\omega_* = 0.5$ for stationary droplets. If $V(0) = 0$, and the control law (8) is assumed, then eq. (3) simplifies to

$$\frac{d\omega}{dt} = \alpha \frac{(\omega_* - \omega)}{(1-G)\partial_\omega \mathcal{N}} \int \sin^2 \Theta d\vec{x}, \quad (10)$$

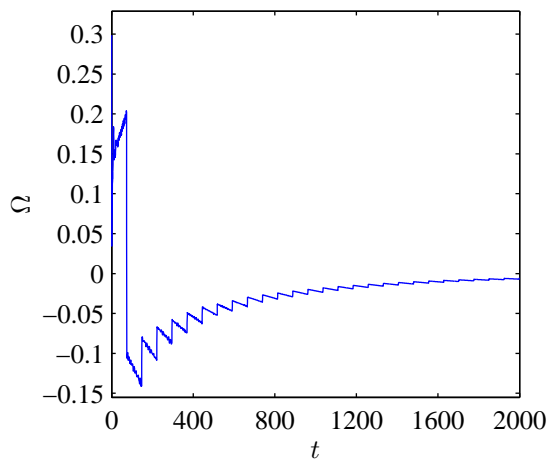


FIG. 5. Micromagnetic simulation giving the spatially averaged magnetization frequency due to the control field (8), $\omega_* = 0.4$, $G = 1.5$, $\alpha = 0.01$, and an update period of 74. The droplet is locked when $\Omega = 0$.

with $V(t) \equiv 0$. Since $\partial_\omega \mathcal{N} < 0$ and $G > 1$, we observe that $\omega = \omega_*$ is a global attractor for fixed $V(t) = 0$ with $\omega(t)$ relaxing monotonically to ω_* .

When $V(0) \neq 0$, the initial state exhibits phase variations leading to droplet propagation. However, as Fig. 4(b) shows, $(\omega, V) = (\omega_*, 0)$ is still an attractor so the phase perturbations decay in time; hence, any drift instability, such as that observed in the case of a nanocontact system¹², has been removed.

We have also performed micromagnetic simulations of eq. (1) incorporating the feedback control law (8). We begin the computation with an asymmetric, localized initial condition

$$\Theta(x, y, 0) = Ae^{-(x/w_x)^2 - (y/w_y)^2}, \quad \Phi(x, y, 0) = 0, \quad (11)$$

where $\vec{m} = (\cos \Phi \sin \Theta, \sin \Phi \sin \Theta, \cos \Theta)$ and $A = 2.7$, $w_x = 2.3$, $w_y = 3$. Equation (1) is evolved with the spatially uniform field (8) where $\omega_* = 0.4$, $\alpha = 0.01$, $G = 1.5$. We “measure” $\Omega(t)$ by averaging the in-plane magnetization orientation over the unit disk to obtain an average phase $\bar{\Phi}(t)$. This models the nanocontact measurement technique suggested; then, $\Omega(t) = \frac{d\bar{\Phi}}{dt}(t)$. We perform computations with differing bandwidths or update times so that $h_0(t)$ is updated instantaneously and periodically. Figure 5 depicts the evolution of the total frequency $\Omega(t)$ with a field update period of 74 time units, which translates to 2 ns or a 500 MHz bandwidth for perpendicular magnets used in recent experiments¹⁸. Because damping drives the dynamics, we expect that the operable control bandwidth is approximately $\alpha|\gamma|\mu_0 M_s(Q - 1)$, corresponding to about 400 MHz. This suggests that any sufficiently large, localized excitation created by spin torque or other means can be deformed into a stationary droplet of choice solely with the use of an external, spatially uniform magnetic field. Physically, this stabilization mechanism balances

the switching of a droplet by a sufficiently negative bias field and the decay of a droplet via damping.

B. Droplet Speed Control

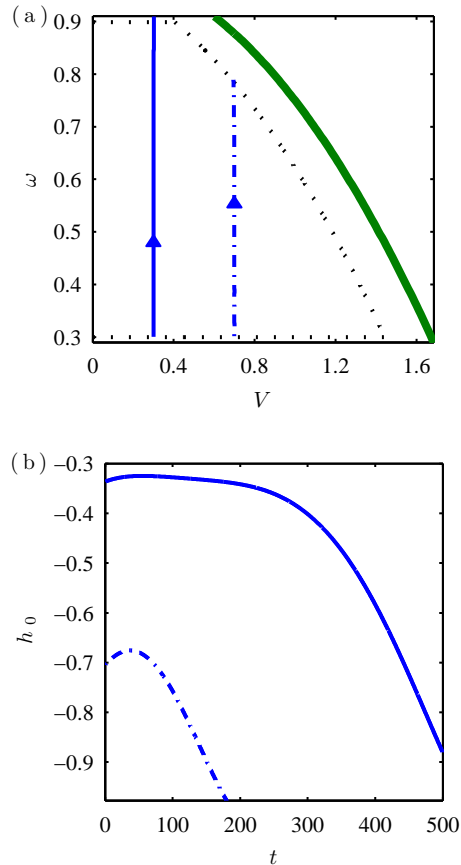


FIG. 6. Open-loop control of droplet speed. (a) Two trajectories (solid, dash-dotted) in the V - ω plane from micromagnetic simulations with (b) the corresponding control field (solid, dash-dotted, respectively) determined from the modulation equations (3).

In the presence of damping and a constant magnetic field, a propagating droplet is either accelerated or decelerated (recall Fig. 2). A time-varying, spatially uniform open-loop control field can be used to stabilize the droplet’s speed. For this, we implement an optimization strategy for the modulation equations (3) by stepping forward in time and determining the field $h_0(t)$ that enforces the constraint of constant speed. The resulting field profile is fit to a quintic polynomial (see Fig. 6(b)) and used in a micromagnetic simulation of eq. (1) resulting in the trajectories shown in Fig. 6(a). Remarkably, the control field from modulation theory leads to accurate control of the droplet’s speed in the full micromagnetic simulation.

VI. CONCLUSION

We have demonstrated that droplets propagating in a realistic, damped ferromagnet can be sustained, accelerated, and controlled by use of only an external magnetic

field. Combining a nanocontact system¹² with the ideas presented here provides a framework to create and control moving droplet solitons in a ferromagnet. Their robustness and controllability hold promise for future spintronic applications.

-
- * mahoefer@ncsu.edu; <http://www4.ncsu.edu/~mahoefer/>
 † msommac@ncsu.edu
 ‡ silva@nist.gov
- ¹ S. Bader and S. Parkin, *Ann. Rev. Cond. Mat. Phys.*, **1**, 71 (2010); J. Lau and J. Shaw, *J. Phys. D: Appl. Phys.*, **44**, 303001 (2011).
 - ² J. C. Slonczewski, *J. Magn. Magn. Mater.*, **159**, L1 (1996); L. Berger, *Phys. Rev. B*, **54**, 9353 (1996).
 - ³ J. Katine and E. E. Fullerton, *J. Magn. Magn. Mater.*, **320**, 1217 (2008).
 - ⁴ T. Silva and W. Rippard, *J. Magn. Magn. Mater.*, **320**, 1260 (2008).
 - ⁵ D. Berkov and J. Miltat, *J. Magn. Magn. Mater.*, **320**, 1238 (2008).
 - ⁶ X. W. Yu, V. S. Pribiag, Y. Acremann, A. A. Tulapurkar, T. Tylizszczak, K. W. Chou, B. Bräuer, Z. Li, O. J. Lee, P. G. Gowtham, D. C. Ralph, R. A. Buhrman, and J. Stöhr, *Phys. Rev. Lett.*, **106**, 167202 (2011).
 - ⁷ J. C. Slonczewski, *J. Magn. Magn. Mater.*, **195**, L261 (1999); M. A. Hoefer, M. J. Ablowitz, B. Ilan, M. R. Puffall, and T. J. Silva, *Phys. Rev. Lett.*, **95**, 267206 (2005); M. A. Hoefer, T. J. Silva, and M. D. Stiles, *Phys. Rev. B*, **77**, 144401 (2008).
 - ⁸ S. Bonetti, V. Tiberkevich, G. Consolo, G. Finocchio, P. Muduli, F. Mancoff, A. Slavin, and J. Åkerman, *Phys. Rev. Lett.*, **105**, 217204 (2010).
 - ⁹ V. E. Demidov, S. Urazhdin, and S. O. Demokritov, *Nat. Mater.*, **9**, 1476 (2010); M. Madami, S. Bonetti, G. Consolo, S. Tacchi, G. Carlotti, G. Gubbiotti, F. B. Mancoff, M. A. Yar, and J. Åkerman, *Nat. Nano.*, **6**, 635 (2011).
 - ¹⁰ A. Slavin and V. Tiberkevich, *Phys. Rev. Lett.*, **95**, 237201 (2005).
 - ¹¹ D. V. Berkov and N. L. Gorn, *Phys. Rev. B*, **76**, 144414 (2007); G. Consolo, B. Azzerboni, G. Gerhart, G. A. Melkov, V. Tiberkevich, and A. N. Slavin, *ibid.*, **76**, 144410 (2007).
 - ¹² M. A. Hoefer, T. J. Silva, and M. W. Keller, *Phys. Rev. B*, **82**, 054432 (2010).
 - ¹³ A. M. Kosevich, B. A. Ivanov, and A. S. Kovalev, *Pis'ma Zh. Eksp. Teor. Fiz.*, **25**, 516 (1977); A. S. Kovalev, A. M. Kosevich, and K. V. Maslov, *JETP Lett.*, **30**, 296 (1979); A. M. Kosevich, B. A. Ivanov, and A. S. Kovalev, *Phys. Rep.*, **194**, 117 (1990).
 - ¹⁴ B. Piette and W. J. Zakrzewski, *Physica D*, **119**, 314 (1998).
 - ¹⁵ B. A. Ivanov, C. E. Zaspel, and I. A. Yastremsky, *Phys. Rev. B*, **63**, 134413 (2001).
 - ¹⁶ M. A. Hoefer and M. Sommacal, *Physica D*, **241**, 890 (2012).
 - ¹⁷ L. F. Mollenauer and J. P. Gordon, *Solitons in optical fibers* (Academic Press, New York, 2006).
 - ¹⁸ W. H. Rippard, A. M. Deac, M. R. Puffall, J. M. Shaw, M. W. Keller, S. E. Russek, G. E. W. Bauer, and C. Serpico, *Phys. Rev. B*, **81**, 014426 (2010); S. M. Mohseni, S. R. Sani, J. Persson, T. N. Anh Nguyen, S. Chung, Ye. Pogoryelov, and J. Åkerman, *Phys. Status Solidi RRL*, **5**, 432 (2011).
 - ¹⁹ F. H. D. Leeuw, R. V. D. Doel, and U. Enz, *Rep. Prog. Phys.*, **43**, 689 (1980).
 - ²⁰ A. A. Thiele, *J. Appl. Phys.*, **41**, 1139 (1970).
 - ²¹ Y. S. Kivshar and B. A. Malomed, *Rev. Mod. Phys.*, **61**, 763 (1989).
 - ²² V. G. Bar'yakhtar, B. A. Ivanov, T. K. Soboleva, and A. L. Sukstanskii, *Sov. Phys. JETP*, **64**, 857 (1986).
 - ²³ A. M. Kosevich, V. V. Gann, A. I. Zhukov, and V. P. Voronov, *JETP*, **87**, 401 (1998); I. M. Babich and A. M. Kosevich, *Low Temp. Phys.*, **27**, 35 (2001).
 - ²⁴ V. G. Baryakhtar and B. A. Ivanov and A. L. Sukstanskii and E. Yu. Melikhov, *Phys. Rev. B*, **56**, 619 (1997).
 - ²⁵ N. R. Cooper, *Phys. Rev. Lett.*, **80**, 4554 (1998).
 - ²⁶ The precomputed droplet library consists of accurately resolved solitons with parameters (V, ω) lying in the set $\{(V, \omega) \mid 0 \leq V \leq 2\sqrt{1-\omega} - 0.25, 0.275 \leq \omega \leq 0.95\}$ ¹⁶.